Issues of Impedance Emulation of Converter-Based Grid Emulator for LVRT Test

Li, Zejie; Zhao, Fangzhou; Chen, Xingxing; Munk-Nielsen, Stig; Wang, Xiongfei

Published in:
APEC 2023 - 38th Annual IEEE Applied Power Electronics Conference and Exposition

DOI (link to publication from Publisher):
10.1109/APEC43580.2023.10131150

Publication date:
2023

Document Version
Publisher's PDF, also known as Version of record

Issues of Impedance Emulation of Converter-Based Grid Emulator for LVRT Test

Zejie Li, Fangzhou Zhao, Xingxing Chen, Stig Munk-Nielsen, Xiongfei Wang
Department of Energy, Aalborg University
Aalborg, Denmark
Email: zl@energy.aau.dk, fzha@energy.aau.dk, xingstarxjtu@163.com, smn@energy.aau.dk, xwa@energy.aau.dk

***Abstract*—A simultaneous change of voltage magnitude and grid impedance may occur during grid faults. To reproduce such impedance variation by converter-based grid emulators, the virtual impedance (VI) control and the virtual admittance (VA) control are two typical approaches. Their dynamics when used with the *L*-filtered grid emulator are evaluated in this paper. Two major issues, i.e., the inaccuracy of emulated low-frequency (<50 Hz) impedance by the VI control, and the adverse interactions between VA control and its inner current control. Simulation and experimental results of an *L*-filtered voltage source inverter confirm the correctness of analysis.**

Keywords—Transient impedance, low-voltage ride-through, virtual impedance, virtual admittance

I. Introduction

Voltage sags and fault clearances are generally accompanied by impedance variation in power grids. Such changes of grid parameters may affect transient dynamics of grid-connected systems, e.g., the overvoltage and low-frequency (<50 Hz) oscillations at the point of common coupling (PCC) [1], [2]. To test the grid-code compliance of grid-connected systems, it is important for converter-based grid emulators to guarantee the accuracy of emulating steady-state low-frequency impedance profile and transient-state impedance variation [3]-[6].

The voltage control (VC) and virtual impedance (VI) with a low-pass filter (LPF) have been commonly adopted for the impedance emulation [4], [7]. It can realize accurate emulation of steady-state low-frequency impedance in the *LC*-filtered grid emulator, which is dependent on the VC parameters [8], but they cannot be readily extended to the *L*-filtered grid emulator. Additionally, the cutoff frequency of LPF may limit the performance of transient-impedance emulation [4].

To avoid using the LPF, the current control (CC) with the virtual admittance (VA) control can be an alternative method for grid emulators [1], [8]. It can achieve accurate emulation of steady-state impedance in a wide frequency range [8]. Yet, the emulation of small or nearly zero impedance is limited by the design of CC loop and the control latency [9].

This paper reviews first the testing capacity requirements of a grid emulator for low-voltage ride-through (LVRT) tests. To fulfill the requirements on emulating transient changes in both voltage and impedance, the issues with the VI control and the VA control are identified based on the impedance modeling of an *L*-filtered converter-based grid emulator. Lastly, the simulation and experimental tests are conducted to validate the correctness of reported issues.

II. System Description

Fig. 1 shows a shunt-impedance-based grid emulator and a converter-based grid emulator. Z_g, Z_1, Z_2 and Z_v are the grid impedance, the series impedance, the fault impedance and the virtual impedance, respectively. In the former, through opening/closing switches S_1 and S_2, the simultaneous change of voltage magnitude and grid impedance can be implemented for the LVRT tests, as shown in Fig. 1(b) [3]. To reproduce the dynamics of the shunt-impedance-based grid emulator, the converter-based grid emulator with an *L* filter is an attractive structure, which can avoid the *LC*-filter resonance and reduce the footprint of ac filters [1], [10].

In the testing guideline FGW TR3, several requirements have been provided for the impedance profile during LVRT tests, as follows [11].

1) The short-circuit ratio (SCR) seen from PCC is at least 2 before the fault occurrence.

2) The fault impedance Z_2 can be zero to realize the voltage sag depth up to 100%.

3) The X/R ratio of Z_g, Z_1, Z_2 must be at least 3.

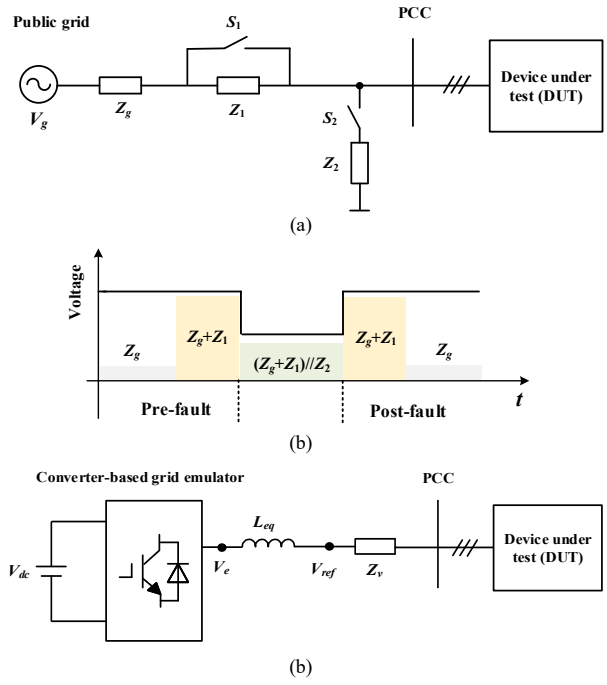

Fig. 1. The general diagram of the grid emulators. (a) Shunt-impedance-based grid emulator. (b) Time sequence of impedance variation. (c) Converter-based grid emulator.

III. Issues of Impedance Emulation

This section elaborates first the limitations of VC with VI control in emulating steady-state low-frequency impedance and transient-state impedance variation. Further, the advantage and adverse interactions of CC with VA control have been discussed.

A. Limitation of VC with VI Control

Fig. 2(a) shows the control diagram of a conventional VC with VI control in the grid emulator with an L filter. $G_d(s)$ and $Z_{op}(s)$ represent the time delay link and the open-loop impedance. $G_v(s)$ and $H(s)$ denotes the VC based on a proportional-resonant (PR) controller and LPF, which can be expressed as

$$G_v(s) = K_{pv} + \frac{K_{rv}s}{s^2 + \omega_1^2} \tag{1}$$

$$H(s) = \frac{\omega_v}{s + \omega_v} \tag{2}$$

where K_{pv}, K_{rv}, ω_1, ω_v are the proportional gain, resonant gain, the fundamental angular frequency and the cutoff angular frequency of LPF.

The open-loop gain of the VC loop is

$$G_{opvc}(s) = \left(K_{pv} + \frac{K_{rv}s}{s^2 + \omega_1^2} \right) e^{-sT_d} \tag{3}$$

where T_d is the time delay.

The gain margin (GM) and phase margin (PM) of $G_{opvc}(s)$ are expressed as

$$\begin{cases} \mathrm{GM}_{vc} \approx -20\lg\left[\sqrt{\left(K_{pv}\right)^2 + \left(\dfrac{K_{rv}}{2\pi f_{cv}}\right)^2} \right] \\ \mathrm{PM}_{vc} \approx \pi - \arctan\left(\dfrac{K_{rv}}{2\pi K_{pv} f_{cv}} \right) - 2\pi f_{cv} T_d \end{cases} \tag{4}$$

where f_{cv} is the phase-crossover frequency of $G_{opvc}(s)$.

To guarantee the internal stability of system, GM_{vc} and PM_{vc} cannot be less than zero. Thus, the boundaries of K_{pv} and K_{rv} are derived as

$$\begin{cases} K_{pv} \le 1 \\ K_{rv} \le \dfrac{\pi}{2T_d} \end{cases} \tag{5}$$

The output impedance of system is given by

$$Z_{GE}(s) = Z_{op}(s) + \frac{G_v(s)G_d(s)}{1 + G_v(s)G_d(s)} \left[Z_v(s)H(s) - Z_{op}(s) \right] \tag{6}$$

where $Z_{op}(s)=sL_{eq}$ and L_{eq} is the equivalent AC inductance.

According to (1) and (5), $G_v(s)$ is close to $K_{pv}\le 1$ in the low-frequency region, which causes $Z_{GE}(s)$ not equal to $Z_v(s)$. As a result, the VC with VI control cannot ensure the accuracy of steady-state low-frequency impedance emulation.

Table I shows system parameters. Fig. 2(b) and Fig. 2(c) depict the bode diagram for output impedance of the grid emulator and ideal impedance. K_{pv}=0 leads to a severe error of emulating steady-state impedance in the low-frequency region, especially for weak-grid emulation. Increasing K_{pv} can enhance the impedance emulation but not eliminate the error. Besides, the cutoff frequency of LPF is usually lower than 1 kHz to avoid the effect of the derivative term in the virtual impedance [4], [7].

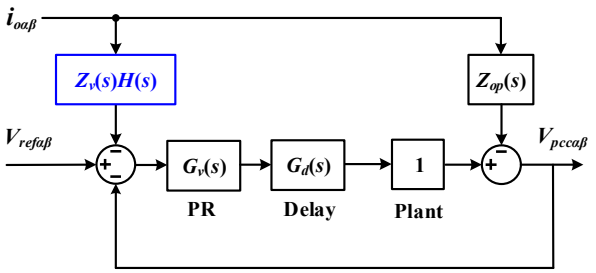

(a)

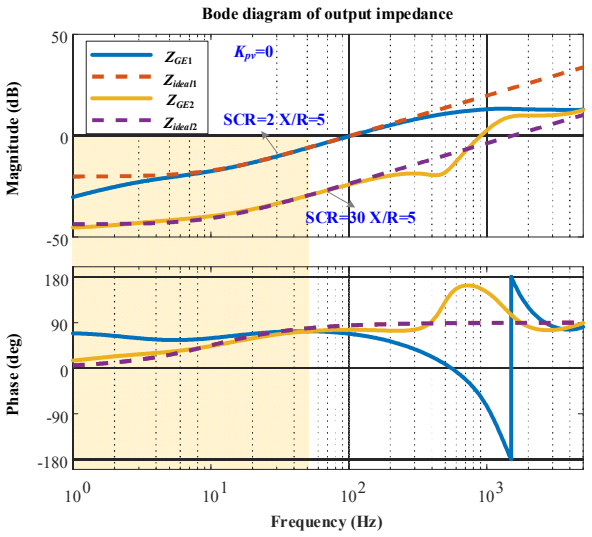

(b)

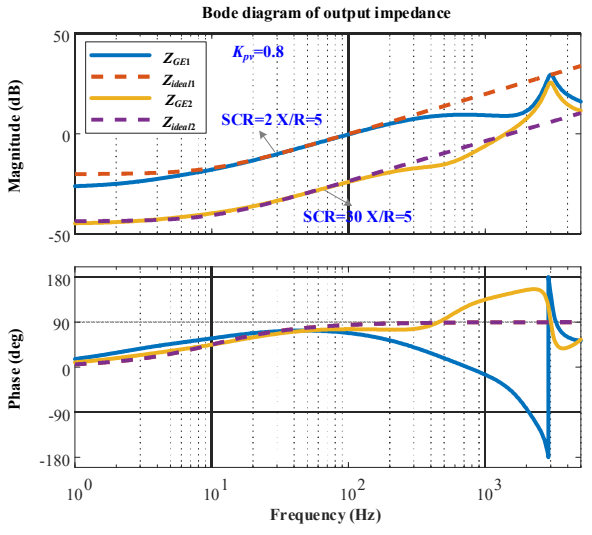

(c)

Fig. 2. The VC with VI control for impedance emulation. (a) Control diagram. (b) Bode diagram of output impedance with K_{pv}=0. (c) Bode diagram of output impedance with K_{pv}=0.8.

Besides, considering transient-impedance emulation during LVRT tests, the LPF may limit the response time of impedance variation. According to (6) and Fig. 1(b), with the increase of impedance difference before and after the emulated voltage sag, the influence of LPF is more adverse.

B. Limitation of CC with VA Control

Fig. 3(a) shows the conventional CC with VA control in the grid emulator with an L filter. $Y_v(s)$ and $G_i(s)$ represent the transfer function of VA and the current controller. The CC is based on a PR controller.

The open-loop gain of the inner CC loop is

$$G_{opcc}(s)=\left(K_{pi}+\frac{K_{ri}s}{s^2+\omega_1^2}\right)\frac{1}{sL_{eq}}e^{-sT_d} \tag{7}$$

where K_{pi} and K_{ri} are the proportional and resonant gain of current controller.

K_{ri} is often designed for the zero-steady state error and shows little phase delay at the phase-crossover frequency f_{ci}, which can be expressed as [12]

$$\frac{K_{ri}}{2\pi f_{ci}}\approx\frac{K_{pi}}{20} \tag{8}$$

The GM and PM of $G_{opcc}(s)$ are given by

$$\mathrm{GM}_{cc}\approx -20\lg\left(\frac{K_{pi}}{2\pi f_{ci}L_{eq}}\right) \tag{9}$$

$$\mathrm{PM}_{cc}\approx\pi-\frac{\pi}{2}-2\pi f_{ci}T_d \tag{10}$$

To ensure $\mathrm{GM}_{cc}\geq 0$ and $\mathrm{PM}_{cc}\geq 0$, K_{pi} should be designed as

$$K_{pi}\leq\frac{\pi L_{eq}}{2T_d} \tag{11}$$

The output impedance is expressed as

$$Z_{GE}(s)=Z_v(s)\frac{Z_{op}(s)+G_i(s)G_d(s)}{Z_v(s)+G_i(s)G_d(s)} \tag{12}$$

According to (11) and (12), K_{pi} can be much greater than 1, which ensures that the steady-state $Z_{GE}(s)$ equals $Z_v(s)$ at low-frequency region, seen in Fig. 3(b).

The open-loop gain of external VA control is

$$G_{opva}(s)=\frac{1}{R_v+sL_v}\left(K_{pi}+\frac{K_{ri}s}{s^2+\omega_1^2}\right)e^{-sT_d} \tag{13}$$

where R_v and L_v are the virtual resistance and inductance.

The GM and PM of $G_{opva}(s)$ are given by

$$\mathrm{GM}_{va}\approx -20\lg\left(\frac{K_{pi}}{2\pi f_{cva}L_v}\right) \tag{14}$$

$$\mathrm{PM}_{va}\approx\pi-\frac{\pi}{2}-2\pi f_{cva}T_d \tag{15}$$

where f_{cva} is the phase-crossover frequency of $G_{opva}(s)$.

The control plant is a unit gain in $G_{opva}(s)$, which results in the interactions between CC and VA control in the grid emulator with L filters. Fig. 3(c) shows the bode diagram of open-loop gain with several emulating impedances.

As the emulating impedance decreases, the PM_v tends to be smaller than zero, causing an internal instability problem. To ensure $\mathrm{GM}_{va}\geq 0$ and $\mathrm{PM}_{va}\geq 0$, the emulating inductance should satisfy

$$L_v\geq\frac{2K_{pi}T_d}{\pi} \tag{16}$$

Thus, the CC parameters and time delay limit the minimum emulating impedance based on VA control.

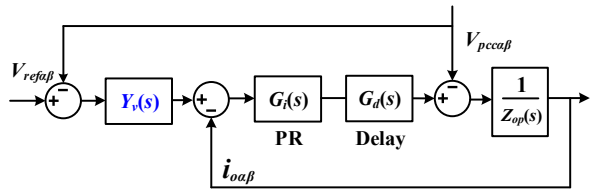

(a)

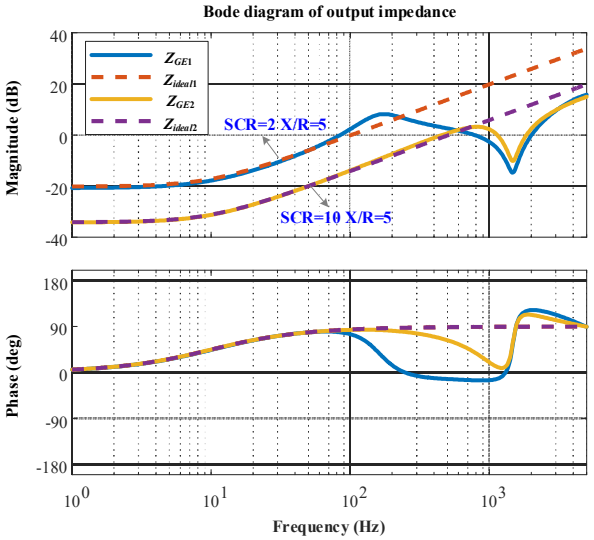

(b)

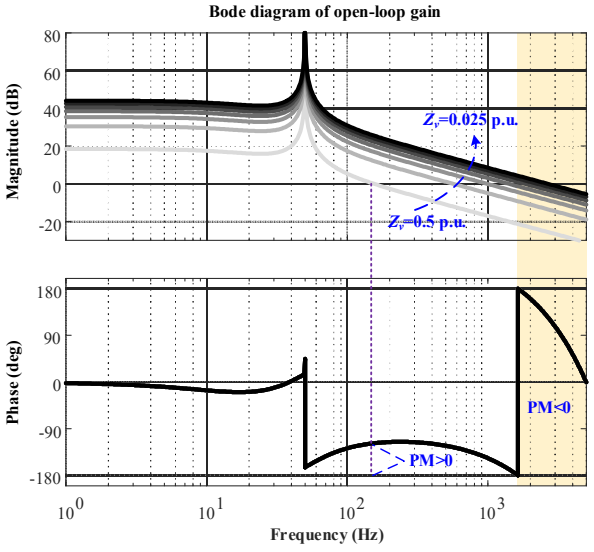

(c)

Fig. 3. The CC with VA control for impedance emulation. (a) Control diagram. (b) Bode diagram of output impedance. (c) Bode diagram of open-loop gain based on fixed CC parameters with different emulating impedances.

Additionally, the cutoff frequency of VA control is lower with the increase of emulating impedance, which weakens the emulating accuracy of transient impedance. Moreover, it is not easy to identify the required bandwidth for VA control due to the nonlinear dynamics during LVRT tests.

IV. Simulation and Experimental Validation

A. Simulation Validation

In respect to the grid emulator with an L filter, the modular multilevel converter (MMC) is taken as an example. A simulation model of an MMC-based grid emulator and a grid-following DUT is established in the PLECS. Table I presents the simulation parameters of grid emulation system.

Fig. 4 shows the simulation results of two impedance control methods. Fig. 4(a) and Fig. 4(b) demonstrate the zero-voltage ride-through (ZVRT) test results under SCR=3 and SCR=2 of emulating grid by the VC with VI control. At SCR=3, compared to the PCC voltage and current of the shunt-impedance-based grid emulator (physical system), the MMC-based grid emulator shows a slight error in emulating steady-state low-frequency impedance and transient-state impedance variation. Nevertheless, as the SCR of emulating grid decreases, the DUT shows a loss of synchronization (LOS) phenomenon which amplifies the inaccuracy of transient-impedance emulation. Moreover, the error of steady-state impedance emulation by VI control is increased. Consequently, the desired oscillation cannot be reproduced by the grid emulator.

Fig. 4(c) illustrates the simulation results of the grid emulator based on the CC with VA control during LVRT test (voltage sags to 0.07 p.u.). When the L_v is lower than identified minimum impedance based on CC with VA control, an internal instability problem indeed occurs.

Fig. 4(d) illustrates the simulation results of the grid emulator based on the CC with VA control during LVRT test (voltage sags to 0.2 p.u.). Although the accuracy of steady-state low-frequency impedance emulation is enhanced, the low-bandwidth VA control doesn't ensure accurate transient-state impedance. It causes different oscillating frequencies during the LOS process between the converter-based grid emulator and the shunt-impedance-based grid emulator.

TABLE I Simulation Parameters of Grid Emulation System

Converters	Symbol	Meaning	Value
Grid emulator	V_{pcc_ll}	PCC voltage (l-l, rms)	11 kV (1 p.u.)
	S_o	Rated power	4 MVA (1 p.u.)
	L_s	Equivalent ac inductance	5 mH (0.05 p.u.)
	f_{sw}	Equivalent switching frequency	10 kHz
	f_{sa}	Sampling frequency	10 kHz
	T_d	Time delay	150 μs
	f_v	Cutoff frequency of LPF	500 Hz
	K_{pv}	Proportional gain of VC	0.8
	K_{rv}	Resonant gain of VC	5000
	K_{pc}	Proportional gain of CC	40
	K_{rc}	Resonant gain of CC	17500
DUT	N_{tr}	Transformer voltage ratio	11 kV/690 V
	L_{tr}	Leakage inductance	10 mH (0.1 p.u.)
	L_{s_DUT}	Inverter inductance	3 mH (0.03 p.u.)
	K_{p_DUT}	Proportional gain of CC	0.35
	K_{i_DUT}	Resonant gain of CC	100
	f_{sa_DUT}	Sampling frequency	10 kHz

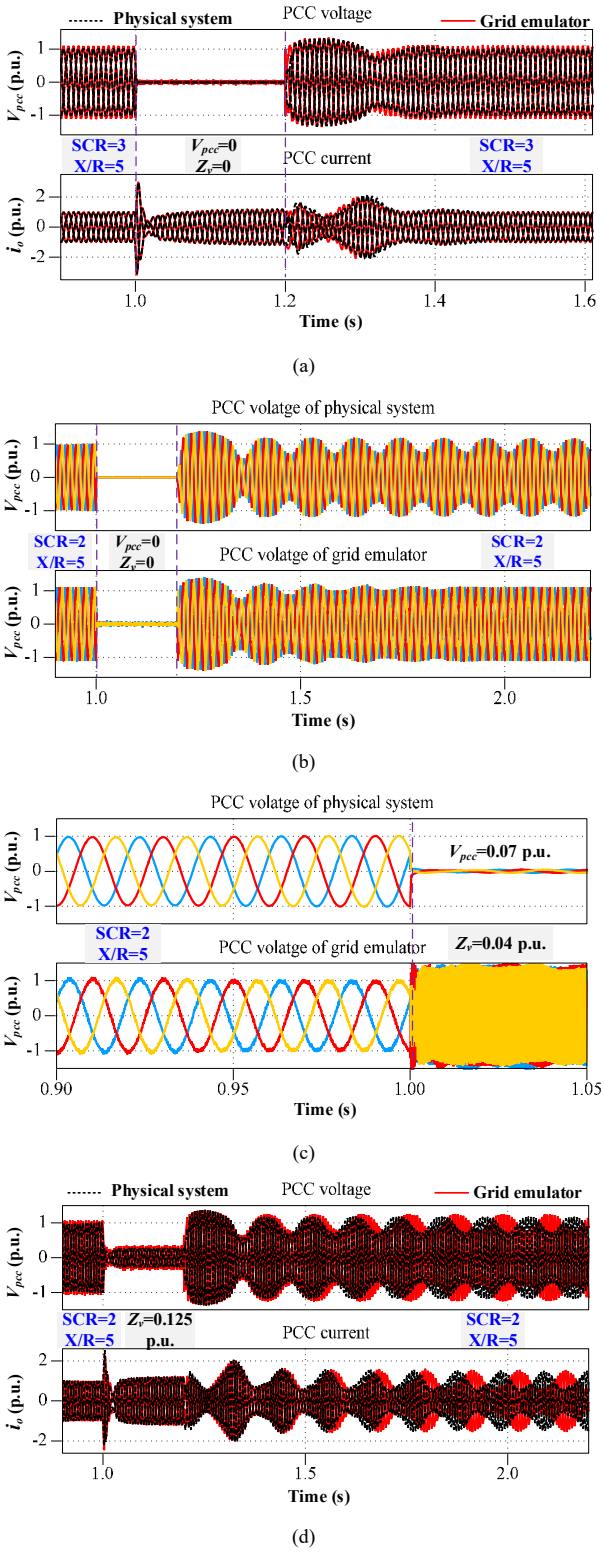

Fig. 4. The simulation results for two impedance control methods. (a) SCR=3 based on VC with VI control. (b) SCR=2 based on VC with VI control. (c) CC with VA control (voltage sags to 0.07 p.u.). (d) CC with VA control (voltage sags to 0.2 p.u.).

B. Experimental Validation

The closed-loop modulation and energy-based balancing control of submodule capacitor voltage have been adopted for the MMC-based grid emulator, which can mitigate the impact of internal dynamics on the external output [13], [14]. Thus, the MMC-based grid emulator can be equivalent to a 2-level voltage source converter (VSC) with an L filter. To simplify analysis, an experimental platform has been built by two back-to-back (BTB) 2-level VSCs, as shown in Fig. 5. Table II shows the down-scaled experimental parameters.

In Fig. 5, the YASKAWA D1000 converter is used as an active front end (AFE) to provide the stable dc-link voltage for the Danfoss inverter. The left-side BTB converter is the grid emulator and the right-side BTB converter is a grid-following DUT. The DUT utilizes the LC filter and the grid emulator adopts the L filter. Further, the transformer of DUT is equivalent to the ac inductor. Besides the power hardware, the control hardware employs the dSPACE-1007 and DS2004 A/D sampling board, which is used to implement the control algorithms of the grid emulator and the grid-following DUT.

Fig. 6 illustrates the experimental results for two impedance control methods. Fig. 6(a) shows the ZVRT test with emulating impedance variation at initial SCR=2 based on the VC with VI control. Similar to Fig. 4(b), the PCC voltage shows several low-frequency (about 8 Hz) oscillations after the voltage recovery instant, then keeps stable operation. It demonstrates that the VC with VI control cannot correctly reproduce the LOS phenomenon due to the limitation of emulating impedance.

Fig. 6(b) shows an LVRT test with Z_v=0.04 p.u. during voltage sag by the CC with VA control. At this case, a large open-loop gain causes the internal instability problem.

TABLE II EXPERIMENTAL PARAMETERS OF GRID EMULATION SYSTEM

Converters	Symbol	Meaning	Value
Grid emulator	V_{pcc_ll}	PCC voltage (l-l, rms)	220 V (1 p.u.)
	S_o	Rated power	1.5 kW (1 p.u.)
	L_s	Equivalent ac inductance	5 mH (0.05 p.u.)
DUT	L_{tr_eq}	Equivalent leakage inductance	10 mH (0.1 p.u.)
	L_{s_DUT}	Inverter inductance	3 mH (0.03 p.u.)
	C_{DUT}	ac capacitance	15 μF

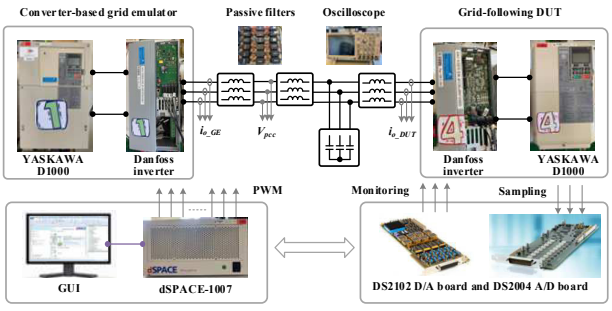

Fig. 5. The experimental platform for the grid emulator and DUT.

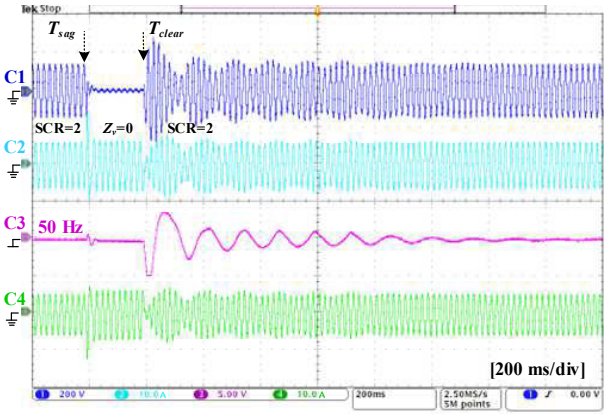

(a)

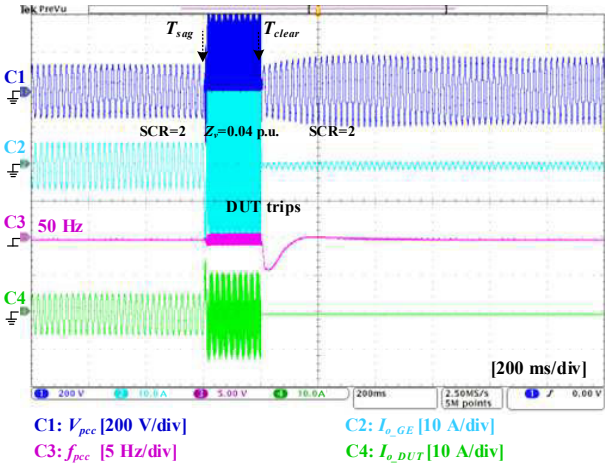

(b)

Fig. 6. The experimental results for two impedance control methods. (a) Emulating impedance based on VC with VI control. (b) Emulating impedance based on CC with VA control.

V. CONCLUSION

This paper figures out the issues of impedance emulation by VC with VI control and CC with VA control in the converter-based grid emulator with an L filter. Simulation and experimental results have confirmed that the inaccuracy of low-frequency (<50 Hz) impedance emulation occurs in the VI control, which results in failing to reproduce the intentional LOS phenomenon. Additionally, there are adverse interactions between CC and VA control, which may cause the inaccuracy of transient-state impedance emulation or even internal instability.

REFERENCES

[1] Z. Li *et al.*, "Testing requirements and control strategies of next-generation grid emulator: a review," in *Proc. IPEC-Himeji 2022-ECCE Asia*, Himeji, Japan, 2022, pp. 1560-1566.

[2] Y. Li *et al.*, "Pll synchronization stability analysis of mmc-connected wind farms under high-impedance ac faults," *IEEE Trans. Power Syst.*, vol. 36, no. 3, pp. 2251-2261, May 2021.

[3] A. Frehn, S. Azarian, G. Quistorf, S. Adloff, F. Santjer, and A. Monti, "First comparison of the electrical properties of two grid emulators for UVRT test against field measurement," *Forschung im Ingenieurwesen*, vol. 85, no. 2, pp. 373-384, 2021.

[4] N. Espinoza, M. Bongiorno, and O. Carlson, "Novel LVRT testing method for wind turbines using flexible VSC technology," *IEEE Trans. Sustain. Energ.*, vol. 6, no. 3, pp. 1140-1149, Jul. 2015.

[5] A. Frehn, R. Grune, H. Röttgers, and A. Monti, "Influence of the grid parameters during under voltage ride through (UVRT) testing," *Forschung im Ingenieurwesen*, vol. 85, no. 2, pp. 559-566, 2021.

[6] S. Azarian, T. Jersch, S. Khan, and S. Azarian, "Comparison of impedance behavior of UVRT container with medium voltage grid simulator in case of unsymmetrical voltage dip," in *Proc. CWD*, Aachen, Germany, 2019, pp. 1-12.

[7] X. Wang, Y. W. Li, F. Blaabjerg and P. C. Loh, "Virtual-impedance-based control for voltage-source and current-source converters," *IEEE Trans. Power Electron.*, vol. 30, no. 12, pp. 7019-7037, Dec. 2015.

[8] J. Wang *et al.*, "Dual-frequency bands grid impedance emulator for stability test of grid-connected converters," *IEEE Trans. Power Electron.*, vol. 37, no. 11, pp. 13070-13080, Nov. 2022.

[9] P. Rodriguez, I. Candela, C. Citro, J. Rocabert and A. Luna, "Control of grid-connected power converters based on a virtual admittance control loop," in *Proc. EPE*, Lille, France, 2013, pp. 1-10.

[10] P. Koralewicz, V. Gevorgian, R. Wallen, W. van der Merwe and P. Jörg, "Advanced grid simulator for multi-megawatt power converter testing and certification," in *Proc. ECCE*, Milwaukee, WI, USA, 2016, pp. 1-8.

[11] FGW TR3, "Bestimmung der elektrischen eigenschaften von erzeugungseinheiten und -anlagen, speicher sowie für deren komponenten am mittel-, hoch- und höchstspannungsnetz," 2018.

[12] X. Wang, P. C. Loh, and F. Blaabjerg, "Stability analysis and controller synthesis for single-loop voltage-controlled VSIs," *IEEE Trans. Power Electron.*, vol. 32, no. 9, pp. 7394-7404, Sep. 2017.

[13] M. Jia, S. Cui, K. Hetzenecker, J. Hu, and R. W. De Doncker, "Control of a three-phase four-wire modular multilevel converter as a grid emulator in fault scenarios," in *Proc. ECCE*, Vancouver, BC, Canada, 2021, pp. 624-631.

[14] L. Harnefors, A. Antonopoulos, S. Norrga, L. Angquist, and H. Nee, "Dynamic analysis of modular multilevel converters," *IEEE Trans. Ind. Electron*., vol. 60, no. 7, pp. 2526-2537, Jul. 2013.